Dynamics of Electron Transfers between Electrodes and Monolayers of Nanoparticles

Jocelyn F. Hicks, Francis P. Zamborini, and Royce W. Murray*

Kenan Laboratories of Chemistry, University of North Carolina CB#3290, Chapel Hill, North Carolina 27599-3290

Received: February 19, 2002; In Final Form: May 22, 2002

This paper describes measurements of the rate of electron transfers between electrodes and attached monolayers of gold nanoparticles (monolayer-protected clusters, MPCs). The Au cores have an average 1.6 nm diameter, and possess a mixed monolayer of hexanethiolate and mercaptoundecanoic acid (MUA) ligands. The nanoparticles are assembled onto Au surfaces coated with a self-assembled MUA monolayer using MUA−carboxylate−zinc ion−MUA−carboxylate bridges. The attached MPC monolayers exhibit well-defined single electron double layer charging voltammetry of the Au cores. The electron-transfer kinetics of the attached nanoparticles are estimated using cyclic voltammetric, alternating impedance, and potential step techniques. Results from these experiments are consistent with one another and yield heterogeneous electron-transfer rates in the range of 40 to 160 s^{-1}.

Introduction

Monolayer-protected gold cluster (MPCs) nanoparticles are both relatively stable and conducive to design and manipulation of the functionality of the protecting monolayer.[1] When dissolved in an electrolyte solution, the metal-like core of the MPC can be electronically charged by, for example, coming into contact with an electrode/electrolyte interface. The MPC is thus like a dissolved capacitor,[1b] whose value is termed its double layer capacitance. When monolayer ligands of the MPC—such as alkanethiolate—provide a low dielectric shell around the core, the individual double layer capacities (C_{CLU}) of the dissolved MPCs are extremely small (sub-aF), so that the voltage intervals (ΔV) of successive one electron double layer chargings of the MPC cores are $> k_BT$ (which at room temperature, expressed in voltage, is 26 mV) and thus experimentally resolvable. In voltammetry of MPCs, either dissolved in electrolyte solutions[2−4] and diffusing to the electrode, or when attached to the electrode surface as monolayers[5,6] or multilayers,[7,8] and bathed in electrolyte solution, the one electron charging steps are detected as a succession of current peaks on the potential axis.[2−4] We have termed this phenomenon quantized double layer (QDL) charging following its discovery[2] in a joint project with the Whetten group. Observing QDL charging requires that an adequate sub-population of the MPC material is mono disperse in capacitance (C_{CLU}) and thus uniformity of ΔV. In the present work the sub-population of MPCs is ca. 30% of the total; MPCs having other C_{CLU} and ΔV values form a continuum background of charging.

Most of the previous work on QDL charging has focused on outlining its thermodynamics, namely on theory and models to account for the voltammetrically observed ΔV spacing for successive one electron charging steps of the MPC cores.[2−4,9a,b] In contrast, although the *dynamics* of electron transfers to/from MPCs are of fundamental importance—being reactions between metal-like objects—there is as yet limited information on the subject. Chen and co-workers have reported on electron transfers between an MPC monolayer tethered directly to an electrode surface via an aromatic dithiolate.[6] We have recently[8] described electron hopping reactions between MPCs in a network polymer film of MPCs coating an electrode (and bathed in electrolyte solution); the measured electron self-exchange rate constant was ca. 10^6 s^{-1} (ca. 10^8 M^{-1} s^{-1}). From electronic conductivities of solid-state samples (no contacting electrolyte solution), MPC^0/MPC^+ electron-transfer rates have been shown to (a) follow a second-order rate law (rate maximizes when $[MPC^0] = [MPC^+]$), (b) vary exponentially with the chain-lengths of the protecting monolayers, and (c) be very large (10^9 to 10^{11} M^{-1} s^{-1}).[10]

In related work, reports[11−13] of metal−insulator−metal electron-transfer reactions at macroscopic mercury[11,13] and gold[12] electrodes separated by thiolate monolayers have enhanced our understanding of this type of electron transfer by outlining[13a] their distance dependencies. These reactions illustrate both "through-bond" as well as "chain-to-chain" processes.[12,13b,c] Experiments performed with STM techniques measuring single molecule resistances[14] and the resistances of monolayers[15] on nanoparticles provide further closely related information.

Additional measurement approaches to nanoparticle electron-transfer dynamics would obviously have value. Attaching MPCs to electrodes by alkane-like connectors offers a strategy for measurement akin to the seminal work of Chidsey,[16a] where otherwise inaccessible rates of electron transfers between an electrode and a redox moiety (ferrocene) were retarded into a tractable range by alkanethiolate bridges. Our connector chemistry for attaching monolayers of MPCs to electrodes is cartooned in Scheme 1. The MUA−carboxylate−zinc ion−MUA−carboxylate linker chain, which potentially serves as an electron-transfer tunneling pathway between the MPC core and electrode, is of substantial length, containing 27 atoms (22 methylene units). Given the exponential dependency between rate and tunneling barrier length, which has[16,17] a decay constant of ca. 1.1/CH_2, the above linker should enormously attenuate the rate of electron transfers between electrode and attached MPC. In Scheme 1, however, the upper portion of the linker chain between MPC core and electrode is unconstrained and thus prone to flexing or coiling (like the "floppy model" of

* Corresponding author.

10.1021/jp025663c CCC: $22.00
Published on Web 07/18/2002

SCHEME 1: Cartoon Outlining Carboxylate−Metal Ion−Carboxylate Bridge Used To Bind MPCs to the Electrode Surface[a]

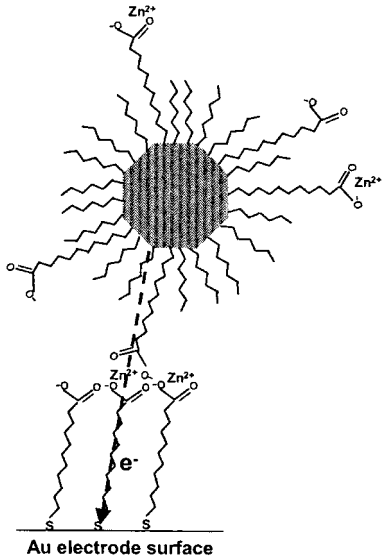

[a] The scheme also depicts an electron-transfer reaction between a gold monolayer-protected cluster (MPC) and the electrode surface. MPC core and ligand size drawn roughly to scale.

earlier chemically modified electrodes[18a−c]). It is conceivable then that reaction occurs through a shorter chain-length pathway than that suggested by the dotted line in Scheme 1. We will conclude below that, for the MPC monolayers, this probably does not occur.

This paper reports measurements of the rates of electron transfers of monolayers of MPCs and the electrodes to which they are attached by the chemistry of Scheme 1. The measurements were carried out with multiple techniques: cyclic voltammetry, potential steps, and ac impedance. All gave similar electron-transfer rate constants. The data reveal some dispersity of electron-transfer rates among the MPC monolayer population, indicative of dispersity in the environments of the MPC population on the electrode surface.

Experimental Section

Synthesis of Mixed Monolayer MPCs. The mixed monolayer MPCs shown in Scheme 1 were prepared starting with synthesis of MPCs with hexanethiolate (C6) monolayers following a modified Brust[19] synthesis. Briefly, the desired thiol and $AuCl_4^-$ were added to toluene in a 3:1 mole ratio and a 10-fold excess of reductant ($NaBH_4$) introduced at 0 °C. The reaction mixture was stirred for 24 h, then the MPC product was recovered by precipitation, filtering, and rinsing with copious amounts of acetonitrile on a glass-fritted Buchner funnel. This MPC product has an average core size of 28 kDa according to laser desorption−ionization mass spectrometry[4] and is denoted C6 MPC.

Mercaptoundecanoic acid (MUA) was ligand-exchanged into the C6 monolayer by stirring tetrahydrofuran (THF) solutions of MPC and the MUA ligand (in selected molar ratios) for ca. 4 days, as reported elsewhere.[20] The mixed monolayer MPC product was collected and washed, like the precursor C6 MPC, and the C6/MUA molar ratio determined by NMR. For the NMR analysis, ligands are quantitatively desorbed from the core as disulfides upon exposure to iodine.[21] The precursor MPCs had an *average* composition[21] of $Au_{140}C6_{53}$ (based on TEM and thermogravimetry data as described previously[21]) and following the ligand exchange, an *average* composition of $Au_{140}C6_{33}(MUA)_{20}$.

Self-Assembled Monolayer (SAM) Formation. Monolayers of mercaptoundecanoic acid (MUA) on Au electrodes were formed by placing a Au disk (Bioanalytical Systems, area 0.02 cm^2) in 2mM MUA in ethanol for >24 h. The Au electrode was first polished with 0.25 μm diamond paste (Buehler), rinsed with distilled and NANOpure water, and cleaned by potential cycling between 1.2 and −0.4 V vs. SCE in sulfuric acid for approximately 3 min.[22]

Attachment of MPCs to Electrodes. Using previously described chemistry,[7] the mixed monolayer C6/MUA MPCs were attached to MUA-functionalized electrodes by successive exposures to ethanol solutions of 1 mM KOH, 0.2 M $ZnNO_3$ (metallating the MUA surface), and 70 μM MPC (plus 10 μL 0.2 M KOH) for 20, 20, and 5 min, respectively. After being removed from each solution the electrode was rinsed copiously with ethanol to remove any MPCs not bound to the electrode surface. These conditions yield approximately a monolayer[23] of attached MPCs (ca. 2×10^{-11} mol/cm^2) as judged by charges under cyclic voltammetric peaks. The clusters can be removed from the electrode surface by placing the electrode in a dilute acid solution.

Measurements. Cyclic voltammetry (CV), differential pulse voltammetry (DPV), and potential step techniques were performed using a Bioanalytical Systems 100B electrochemical analyzer, on Au/MPC films in a 0.1 M Bu_4NPF_6/CH_2Cl_2 electrolyte solution, in a single compartment cell containing Au disk working, $Ag/AgNO_3$ reference, and Pt flag counter electrodes. Alternating current impedance (AC) measurements were obtained using a Solatron 1287 Potentiostat coupled to a Solatron 1255 Impedance/Gain Phase Analyzer. In all cases, background experiments on the MUA-modified Au electrode were taken, prior to MPC exposure.

Results and Discussion

The monolayers of MPCs were attached to the electrode as described in the Experimental Section. Care was taken to constrain the attachment chemistry to a monolayer (MPC multilayers can be generated by changing the attachment reaction conditions[8]) so that the electron-transfer event measured is that of the structure in Scheme 1. Typical cyclic voltammetry and differential pulse voltammetry of the attached MPCs are shown in Figure 1. The coverage of attached MPCs assessed from the charge under the shaded current peak (which is assigned to the Au_{140} $MPC^{2+/1+}$ charge state change) in the Figure 1A cyclic voltammogram is ca. 1×10^{-11} mol/cm^2 which is somewhat less than a monolayer according to an estimate[23] ($1-2 \times 10^{-11}$ mol/cm^2) from a quartz crystal microbalance (QCM) study of MPC adsorption from solution onto naked Au electrodes. The coverage of MPCs assessed using the *total* charge under the current peak (hatched area), is about 3-fold larger, and slightly larger than the QCM determination. We conclude that the MPC attachment conditions successfully limit the MPC film to a monolayer with perhaps a fractional second layer.

The potential of zero charge of surface-attached MPCs is ca. −0.2 V.[5b] This is the basis of labeling the charge state changes of the MPC monolayer shown in Figure 1B. At the peak current for the $MPC^{2+/1+}$ charge state change, the MPC monolayer contains equal quantities of MPCs with Au cores that are neutral and that have lost a single electron. The current peaks in the differential pulse voltammogram in Figure 1B have an average

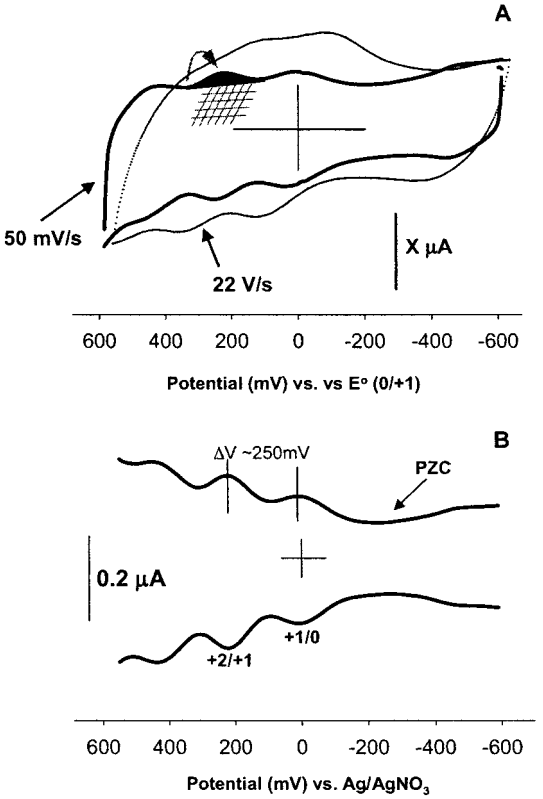

Figure 1. (A) Cyclic voltammetry (CV) of a monolayer of $Au_{140}C6_{33}$-$(MUA)_{20}$ MPCs at potential sweep rates of (—) 50 mV/s where X = 0.1 μA, and (•••) 22 V/s where X = 18 μA, in 0.1 M Bu_4NPF_6 in dichloromethane (CH_2Cl_2). The potential scale is normalized to the formal potential of the $MPC^{0/1+}$ charge state change. Arrow illustrates a potential step performed in the potential step (PS) experiment. MPC coverage ca. 1×10^{-11} mol/cm^2 from the shaded area under the $MPC^{2+/1+}$ current peak; coverage is ca. 2.6×10^{-11}using the hatched area, which besides the working electrode background current, includes the double layer charging current for poly-disperse components of the MPC sample. (The latter produce a featureless current envelope.) (B) Differential Pulse Voltammogram (DPV) of the same film as in (A). Arrow at ca. − 0.2 V indicates potential of zero charge (PZC).

potential spacing $\Delta V = 0.25$ V which corresponds to an average MPC capacitance (C_{CLU}) of ca. 0.64 aF/MPC. This value is near that (~0.6 aF) observed in the solution voltammetry of the same MPCs. Previous experience[6] indicates that attaching MPCs to surfaces does not significantly alter their quantized double layer charging (QDL) properties.

Cyclic Voltammetric Measurement of Electron-Transfer Rates. Cyclic voltammetry is a classical method[17b−f24] for electron-transfer rate determinations and is based on how the separation on the potential axis (ΔE_{PEAK}) of the oxidation and reduction current peaks varies with potential sweep rate (υ). As sweep rate increases so that the time spent traversing the current peak approaches the time scale of the electron-transfer process, the reaction departs from Nernstian behavior, i.e., becomes quasi-reversible, and ΔE_{PEAK} increases. The voltammograms in Figure 1A show that the ΔE_{PEAK} values of the $MPC^{1+/0}$ and $MPC^{2+/1+}$ charge state changes both increase with υ. That of the $MPC^{1+/0}$ couple is the better defined of the two and the individual experimental E_{PEAK} values (● and ■) are plotted in Figure 2. These raw E_{PEAK} values were corrected (symbols ▲) for R_{UNC} using the simple expression $E_{ACTUAL} = E_{PEAK} - i_{PEAK} \cdot R_{UNC}$. Figure 2 illustrates the over-potential induced shift of the oxidation and reduction peak potentials to more negative and positive potentials, respectively.

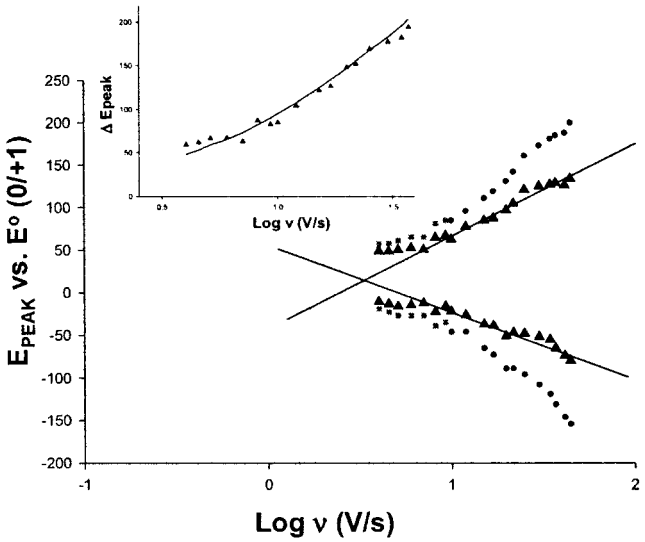

Figure 2. Plot of cyclic voltammetric peak potentials (E_{PEAK}) vs. log-(ν). (—) linear regression at largest potential scan rates (ν), through data for which ΔE_{PEAK} tends toward 200 mV and larger. (● and ■) raw experimental data; (▲) experimental data corrected for R_{UNC} by using the expression $E_{ACTUAL} = E_{PEAK} - i_{PEAK} \cdot R_{UNC}$. $R_{UNC} = 2000\ \Omega$ based on AC impedance results in Figure 4. Using the corrected data, $\alpha = 0.5$ and $k_{ET} = 100\ s^{-1}$. Inset: plot of ΔE_{PEAK} vs log ν and solid line predicted theoretically[25] using $k_{ET} = 100\ s^{-1}$ and $\alpha = 0.5$.

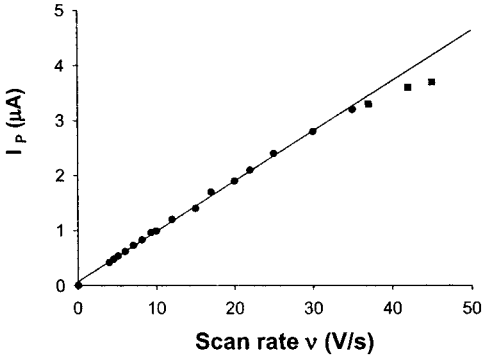

Figure 3. Graph of peak current vs potential scan rate for the $MPC^{1+/0}$ charge state change, for network polymer film shown in Figure 1A. Data (■) are at potential scan rates at which the reaction has become decidedly quasi-reversible.

The variation of peak currents with potential sweep rate for the $MPC^{1+/0}$ charge state change is shown in Figure 3. A linear relation is seen at lower sweep rates as expected for a surface confined electron-transfer process, but at larger sweep rates the plot becomes nonlinear. The nonlinearity is symptomatic of quasi-reversibility, occurs at ca. 30 V s^{-1}, and is qualitatively expected when the reaction becomes charge-transfer rate-limited on the time scale of the potential sweep.

The results in Figure 2 can be analyzed using relations derived by Laviron[24] for chemisorbed electroactive monolayers, and which are most valid when $\Delta E_{PEAK} > 200$ mV (For the raw experimental data, these are the ● points in Figure 2). There, the slopes of linear regressions of oxidation and reduction peak potentials should equal $-2.3RT/\alpha nF$ and $2.3RT/(1-\alpha)nF$, respectively, where α is the electrochemical transfer coefficient. Using the thus derived value of α, the heterogeneous electron-transfer rate (k_{ET}, s^{-1}) can be calculated from

$$\log k_{ET} = \alpha \log(1-\alpha) + (1-\alpha)\log \alpha - \log(RT/nF\nu) - \alpha(1-\alpha)nF\,\Delta E_{PEAK}/2.3RT \quad (1)$$

TABLE 1: k_{ET} and Other Parameters from Fitting of AC Impedance Results

DC potential (mV)[a]	k_{ET} (s^{-1})	C_{ADS} (F)[b,d]	R_{CT} (Ω)	C_{DL} (F)[c,d]
200	89	1.4×10^{-6}	3960	1.6×10^{-7}
200	99	1.0×10^{-6}	4960	2.6×10^{-7}
−70	134	1.4×10^{-6}	2610	3.6×10^{-8}
−70	160	5.6×10^{-7}	5620	2.0×10^{-7}

[a] Potentials referenced to that of $MPC^{1+/0}$ charge state change; see Figure 1A. [b] Exponents (Ψ) used in fitting analysis of constant phase elements were, from top to bottom, 0.8, 0.8, 0.7, and 0.8, respectively. [c] Exponents (Ψ) used in fitting analysis of constant phase elements were, from top to bottom, 0.9, 0.8, 1.0, and 0.9, respectively. [d] Both pseudocapacitance and double layer capacitances were treated as constant phase elements (CPE) in order to achieve the best fit. The impedance of the CPE is described by eq $1/(C(i\omega^{\Psi}))$ where C is capacitance, ω angular frequency, and Ψ an exponent with value between 0 and 1. The closer the value of Ψ to 1, the closer the CPE element is to an ideal capacitor. Deviations from ideality are often attributed to surface roughness.[30]

The regression lines shown in Figure 2 for R_{UNC}-corrected data (▲) give $\alpha \sim 0.45$ and a corresponding k_{ET} value of $\sim 100\ s^{-1}$. (Using the R_{UNC} correction has only a minor effect on the k_{ET} results; see footnote Table 2). Figure 2 (inset) compares E_{PEAK} results for smaller ΔE_{PEAK} values to a theoretical line for $k_{ET} = 100\ s^{-1}$ and $\alpha = 0.5$, using a Table in ref 24. The fit with the experimental points is excellent.

AC Impedance. Alternating current impedance measurements are a powerful approach to electron-transfer dynamics, and have been recently exploited by several laboratories[26] to measure electron-transfer kinetics of surface immobilized redox systems. The experiment rests on applying a small amplitude AC potential (superimposed on a selected DC working electrode potential), and measuring AC current amplitude and phase (with respect to voltage) as a function of the AC potential frequency. The AC current is vectorially decomposed into components that are in-phase (Z', the resistance element) and 90° out-of-phase (Z'', capacitance element).

AC impedance results for a monolayer of $Au_{140}C6_{33}(MUA)_{20}$ MPCs are shown in Figure 4. The frequency range employed is 1.6×10^4 to 16 Hz; data points from left to right correspond to decreasing frequency. Curve A is a "blank", being the response of a Au electrode bearing only a self-assembled MUA monolayer. The response (···) is a semicircle with width (on the Z' axis) corresponding to the solution uncompensated resistance. (The capacitance component of this high-frequency semicircle is probably stray capacitance in the cell in parallel with the resistance. This portion of the data was not used in our analysis, other than to determine the R_{UNC} which can also be taken as the beginning of Curve B.)

Figure 4, Curve B (—) is the response of the $Au_{140}C6_{33}(MUA)_{20}$ monolayer, which at high frequency replicates the uncompensated solution resistance semicircle (at left), and reveals a second, partial semicircle (at right) at lower frequency that we interpret as the resistance to charge-transfer R_{CT} between MPC and electrode. The partial semicircle (Curve B) was fit[27] to the Randles equivalent circuit, starting from $Z' \sim 2000$ (Figure 4 inset, values in figure legend). The uncompensated solution resistance (R_{UNC}) was taken from the Z' axis width of the left-hand semicircle intercept and the adsorption pseudocapacitance (C_{ADS}) from[26a]

$$C_{ADS} = (F^2 A\Gamma)/(4RT) \qquad (2)$$

where F is Faraday's constant, A the electrode area, and Γ the

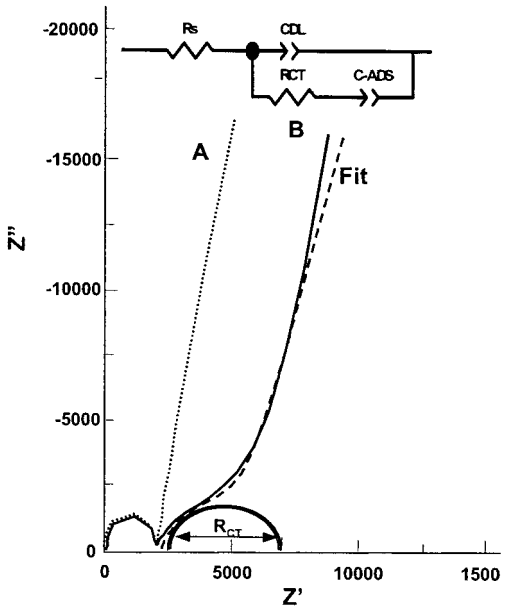

Figure 4. Complex plane impedance plot for a monolayer of $Au_{140}C6_{33}(MUA)_{20}$ MPCs at a dc potential of 0.02 V, AC amplitude 10 mV, and frequency range 16 to 16000 Hz. 0.1 M Bu_4NPF_6 in CH_2Cl_2, E vs. $Ag/AgNO_3$ reference, coverage ca. 1×10^{-11} mol/cm^2. (A) (····) Au electrode with only self-assembled monolayer of MUA; (B) (—) a monolayer of $Au_{140}C6_{33}(MUA)_{20}$ MPCs attached to surface; (- - -) best-fit line over frequency range 16 to 16000 Hz. Inset: equivalent circuit used in fitting analysis, where R_{CT} is resistance to charge transfer (4960 Ω estimated from the right-hand semicircle on the Z' axis), C_{ADS} is pseudo-adsorption capacitance (1.0×10^{-6} F), C_{DL} is double layer capacitance (2.6×10^{-7} F), and R_{UNC} is uncompensated solution resistance (2044 Ω).

MPC coverage per unit area (ca. 1×10^{-11} mol/cm^2). The charge-transfer resistance (R_{CT}) and double layer capacitance (C_{DL}) producing the best fit (— — —) to Curve B in Figure 4 are given in the figure legend. The electron-transfer rate constant is calculated from[26a]

$$k_{ET} = 1/(2R_{CT}C_{ADS}) \qquad (3)$$

Table 1 presents results for several experiments for rate, resistance, and pseudocapacitance parameters. We see that the AC results for the electron-transfer rate k_{ET} agree within a factor of 2 with the cyclic voltammetric results. The two dc potentials tested at 0.2 and −0.07 V were "on" and "off" a charging peak, and as Table 1 shows, the resulting charge transfer resistances have similar values. Ideally, the latter should be larger. We interpret this effect as reflecting the polydispersity of the surface-attached MPC population that does not display visible charging peaks. Finally, we note that the AC impedance method has the virtue of explicitly separating uncompensated solution from charge-transfer resistance. Figure 4 shows that R_{UNC} is within a factor of 2 of R_{CT}, meaning that this rate measurement just narrowly lies within the range of possibility for the particular cell configuration employed.

Potential Step Measurements of Rate Constants. Current−time responses of surface-confined redox substances to potential steps provide information[16,17b] about electron-transfer rates, and also inform as to whether all the species in an immobilized monolayer have the same or a dispersity of rate constants. This experiment moreover, connects the cyclic voltammetry and AC impedance measurements by responding to electron transfers over a range of time scales in a single experiment. Potential steps were executed on electrodes bearing attached monolayers of $Au_{140}C6_{33}(MUA)_{20}$ MPCs, stepping the potentials over the

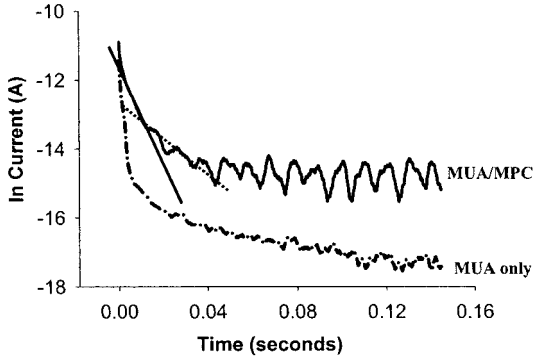

Figure 5. ln *I* vs *t* (current vs time) plots of potential step shown by the arrow in Figure 1A, (- · -) MUA, (—) MUA, and MPC. Lines indicate approximate slopes used to estimates of k_{ET} (—) 150 s^{-1}, and (- - -) 49 s^{-1}, for the shorter and longer portions of the decay.

MPC charging peaks as illustrated by the curved arrow in Figure 1. In that example, the charge state of the MPC core is changed from MPC^{2+} to MPC^{1+} and the final over-potential applied, relative to the $MPC^{1+/2+}$ formal potential, is small. The rate at which the current decays is related to the rate of electron transfer, according to[16a]

$$I = I_o e^{-k_{ET}t} \tag{4}$$

where k_{ET} is the heterogeneous electron-transfer rate (s^{-1}), *t* is time, and I_O is current at time zero. Ideally, for a reaction of a kinetically uniform surface population, a plot of ln *I* versus time is linear with slope of k_{ET}.

An example result (complete with line noise) for a monolayer of attached $Au_{140}C6_{33}(MUA)_{20}$ MPCs is shown in Figure 5 (upper curve). The ln *I* vs *t* response for the MPC monolayer is severely curved. Its slopes yield a range of rate constants, from 50 s^{-1} to 150 s^{-1}, as shown by the regression lines in Figure 5. Curvature of ln *I* vs *t* plots is usually interpreted as kinetic dispersity.[17b] The lower curve in Figure 5 is a potential step performed on a "blank" MUA monolayer; the currents are, as expected, smaller and decay with a much faster time constant.

Potential step experiments were also carried out stepping between the valleys bordering charging peaks (250 mV steps), from a valley to the peak potential (~100 mV steps), and steps from valleys of intermediate size (~150 to 175 mV steps). Ideally, the current−time decay constants should vary systematically with the applied over-potential, i.e., slowest at a current peak potential and largest at one in the current valley, as has been seen for surface immobilized redox species.[16,17b−f] The MPC kinetics did not, however, display any significant variation with applied over-potential, at least that could be discerned given the kinetically disperse response of Figure 5. Examining this result, we noted in the Introduction, and previously,[4] that the samples of Au_{140} MPC nanoparticles we use are not perfectly monodisperse. They do contain a sufficient sub-population of clusters to produce observably discrete QDL charging peaks such as those in Figure 1, but also contain a dispersity of MPC sizes and consequently values of C_{CLU}. The peak potentials for MPC charge state "couples" (e.g., $MPC^{1+/0}$) are, as noted above, separated from one another by potentials ΔV that are governed by their double layer capacitance ($C_{CLU} = 0.64$ aF/MPC). C_{CLU} is in turn is governed[2,3,9] by the MPC core size (and possibly other factors). Double layer charging of a poly-disperse mixture of MPC core sizes, with their distributions of ΔV spacings, formal potentials, and corresponding C_{DL} values, thus yields an unresolved summation of current peaks, which produces the continuum of background current in Figure 1A. In potential step experiments then, each member of a disperse MPC population will undergo electron transfers at a rate governed by the relationship of the applied potential to its own formal potential value. The free energy dependency of any particular MPC population, including that giving the current peaks of Figure 1, is thereby, unfortunately, blurred out. Additional possible sources of kinetic dispersity are noted below.

TABLE 2: Summary of k_{ET} Values

technique	k_{ET} (s^{-1})
cyclic voltammetry	100[a]
potential step	40−150
AC impedance	90−160

[a] Use of E_{PEAK} data uncorrected for R_{UNC} (Figure 2 ●) gives $\alpha = 0.7$ and $k_{ET} = 48$ s^{-1}.

Consideration of the charges passed in potential step experiments is consistent with the preceding analysis. Integrating current−time responses such as that in Figure 5 yields an overall MPC coverage of ca. 3×10^{-11} mol/cm^2. In contrast, the charge under the $MPC^{2+/1+}$ current peak in Figure 1A corresponds to a coverage of ca. 1×10^{-11} mol/cm^2, i.e., this MPC population is only about 1/3 of the total. This result agrees with the relative sizes of the current peaks and the underlying current continuum in Figure 1A.

Consideration of the Kinetic Results. This section presents an overall assessment of the monolayer MPC kinetic measurements, their limitations, and a comparison to other kinetic results.

It is gratifying that the electron-transfer rate constants obtained from the three kinetic methods (Table 2) are in good agreement with one another. Further, each electrochemical methodology supplies particular insights. In the AC impedance experiments, the explicit treatment of the uncompensated resistance excludes distortion from this quarter of the values of rate constants. Analysis of the current−time responses in potential step experiments shows that the overall population of surface-attached MPCs is kinetically quite disperse. The cyclic voltammetric rate determination, on the other hand, is explicitly based on the kinetic behavior of the sub-population of MPCs that produces the current peaks, as opposed to the over-lapping agglomeration of applied over-potentials in the MPC mixture, discussed above for the potential step and AC impedance experiments. That the 10^2 s^{-1} cyclic voltammetric result agrees with the others shows that the kinetic determinations have significance despite the imperfect mono-dispersity of the MPC sample. A similar conclusion about averaging of dispersity effects was drawn in an earlier comparison.[17e]

The dispersity in electron-transfer rate constants (i.e., Figure 5) may not be solely due to the dispersity in MPC formal potentials discussed above, since there may also be structural dispersity within the MPC monolayer (such as nontrans methylene geometries) and multiple electron-transfer pathways. Scheme 2 illustrates possible structural dis-organization of the MPC monolayer and also shows different bonded and nonbonded electron tunneling pathways. The bonded pathway (at left, via the metal coordination) has a chainlength equal to that in Scheme 1 (total of 22 CH_2 units plus the carboxylate/metal ion/carboxylate bridge), and the nonbonded pathway−made possible by folding/coiling of the linker chain−a length of 17 carbon units (including the CH_3) plus the MUA CO_2H group.

Some insight into the probable tunneling pathway in monolayers of surface-attached $Au_{140}C6_{33}(MUA)_{20}$ MPCs can be derived from a comparison to two previous MPC electron-transfer kinetic studies. In one study,[8] the electron-transfer rate constant (ca. 10^6 s^{-1}) between MPC nanoparticles (i.e., electron

SCHEME 2: Monolayer of $Au_{140}C6_{33}((MUA)_{20}$ MPCs Attached to a MUA Functionalized Au Electrode[a]

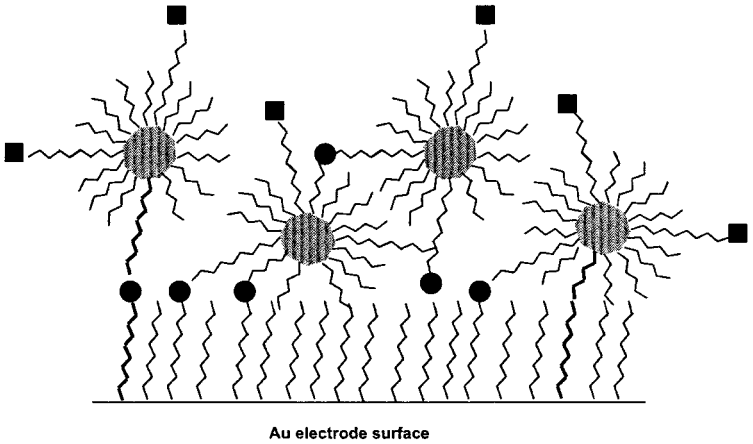

[a] Scheme illustrates differing positions of MPC on MUA monolayer. (●) denotes linker sites, and (■) an acid-terminated ligand. Bold lines at left and right indicate possible "bonded" and "non-bonded" electron tunneling pathways, respectively.

hopping) was measured in a network polymer film in which the MPCs were bonded to one another by chemistry analogous to that in Scheme 1. The MPC network polymer was contacted by a CH_2Cl_2/0.1M Bu_4NPF_6/CH_2Cl_2 electrolyte solution, as is the monolayer of MPCs in the present experiments. More recent results[28] have revealed that electron hopping rates increase when the MPC network polymer is less well swollen. In another study of solid state (solvent-free) alkanethiolate-protected MPCs, nonbonded separation of MPC cores by the equivalent of 12 CH_2 units gave a 10^6 s^{-1} electron hopping rate. These results are the basis of our working hypothesis that in the network polymer, owing to the flexibility of the MPC linkers, the 10^6 s^{-1} MPC-to-MPC electron hopping rate corresponds to tunneling through nonbonded contacts between the *nonlinker* hexanethiolate ligands.

If the above hypothesis is correct, the following analysis shows that, in reference to Scheme 2, reactions of the MPC monolayer via the *bonded* pathway become more plausible. One can estimate[29] for the bonded and nonbonded tunneling pathways illustrated in Scheme 2, that the electron-transfer rate between the electrode and the MPC monolayer should be factors of ca. 8×10^4 and 3×10^2 slower, respectively, than those in the MPC network polymer, or rate constants of ca. 1×10^2 s^{-1} and 3×10^4 s^{-1}, respectively. The experimental finding of ca. 10^2 s^{-1} suggests that the dominant tunneling pathway in the MPC monolayers is the *bonded* linkage shown in Schemes 1 and 2.

It must be stressed that a) while the above results comprise the most complete assessment of nanoparticle monolayer electron-transfer kinetics yet available, b) the current results allow only a crude assessment of structural elements of the MPC monolayer electron-transfer dynamics. We have attempted further measurements in which the ligand chainlengths in MPC monolayers have been varied, but these have not been quantitatively successful, although the qualitative changes are as expected. Thus, attaching the same monolayer of $Au_{140}C6_{33}$-$(MUA)_{20}$ MPCs used above, to an electrode bearing a (longer chainlength) $-S(CH_2)_{15}CO_2H$ self-assembled monolayer, slows the electron transfer as evidenced by increased ΔE_{PEAK} in cyclic voltammetry. Quantitating the kinetic results of such experiments has however been unsatisfactory. A monolayer of MPCs attached to an electrode bearing a MUA self-assembled monolayer, where the linker chain on the MPC was much shorter, 1-mercaptopentanoic acid, gave the AC impedance results shown in Figure 6. Now, the uncompensated resistance semicircle is the same as in Figure 4, but the electron-transfer

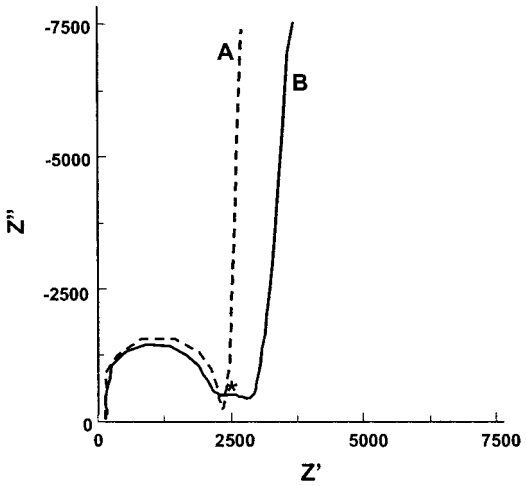

Figure 6. AC Impedance plot for a monolayer of $Au_{140}C6_{33}(MUA)_{20}$ MPCs at a dc potential of 0.1 V. (Note that the charging peaks in this experiment are not exactly at the same values as in Figure 1), AC amplitude 10 mV. 0.1 M Bu_4NPF_6 in CH_2Cl_2, potential vs $Ag/AgNO_3$ reference, Pt flag counter electrode, coverage ca. 2×10^{-11} mol/cm^2. (- - -) MUA only on the surface, (—) redox reaction of MPCs attached to surface. (∗) denotes partially formed semicircle corresponding to the heterogeneous electron-transfer event.

resistance has diminished to a barely perceptible value that is crudely estimated as a rate constant of 5×10^3 s^{-1}. This result, relative to the 10^2 s^{-1} result for the monolayer of Scheme 1, MPC, is consistent with a 7 CH_2 unit decrease in the length of the tunneling pathway.

Acknowledgment. This research was supported in part by grants from the National Science Foundation and the Office of Naval Research.

References and Notes

(1) Templeton, A. C.; Wuelfing, W. P.; Murray, R. W. *Acc. Chem. Res.* **2000**, *33*, 27−36. (b) Green, S. J.; Pietron, J. J.; Stokes, J. J.; Hostetler, M. J.; Vu, H.; Wuelfing, W. P.; Murray, R. W. *Langmuir* **1998**, *14*, 5612.

(2) Ingram, R. S.; Hostetler, M. J.; Pietron, J. J.; Murray, R. W.; Schaaff, T. G.; Khoury, J.; Whetten, R. L.; Bigioni, T. P.; Guthrie, D. K.; First, P. N. *J. Am. Chem. Soc.* **1997**, *119*, 9279.

(3) Chen, S.; Ingram, R. S.; Hostetler, M. J.; Pietron, J. J.; Murray, R. W.; Schaaff, T. G.; Khoury, J.; Alvarez, M. M.; Whetten, R. L. *Science* **1998**, *280*, 2098.

(4) Hicks, J. F.; Templeton, A. C.; Chen, S.; Sheran, K. M.; Jasti, R.; Murray, R. W.; Debord, J.; Schaaff, T. G.; Whetten, R. L. *Anal. Chem.* **1999**, *71*, 3703.

(5) Chen, S.; Murray, R. W. *J. Phys. Chem. B* **1999**, *103*, 682. (b) Chen, S.; Murray, R. W. *J. Phys. Chem. B* **1999**, *103*, 9996.

(6) Chen, S. *J. Phys. Chem.* **2000**, *104*, 663.

(7) Zamborini, F. P.; Hicks, J. F.; Murray, R. W. *J. Am Chem. Soc.* **2000**, *122*, 4515.

(8) Hicks, J. F.; Zamborini, F. P.; Osisek, A. J.; Murray, R. W. *J. Am. Chem. Soc.* **2001**, *123*, 7048.

(9) Chen, S.; Murray, R. W.; Feldberg, S. W. *J. Phys. Chem. B* **1998**, *102*, 9898. (b) Riemers, J. R.; Hush, N. S. *J. Phys. Chem.* **2001**, *105*, 8979.

(10) (a) Wuelfing, W. P.; Green, J. J.; Cliffel, D. E.; Pietron, J. P.; Murray, R. W. *J. Am. Chem. Soc.* **2000**, *122*, 11465. (b) Wuelfing, W. P.; Murray, R. W. *J. Phys. Chem.*, in press.

(11) (a) Haag, R.; Rampi, M. A.; Holmlin, R. E.; Whitesides, G. M. *J. Am. Chem. Soc.* **1999**, *121*, 7895. (b) Holmlin, R. E.; Haag, R.; Chabincy, M. L.; Ismagilov, R. F.; Cohen, A. E.; Terfort, A.; Rampi, M. A.; Whitesides, G. M. *J. Am. Chem. Soc.* **2001**, *123*, 5075.

(12) (a) Zhou, C.; Deshpande, M. R.; Reed, M. A.; Jones, L.; Tour, J. M. *Appl. Phys. Lett.* **1997**, *71*, 611. (b) Reed, M. A.; Zhou, C.; Muller, C. J.; Burgin, T. P.; Tour, J. M. *Science* **1997**, *278*, 252.

(13) (a) Slowinski, K.; Fong, H. K. Y.; Majda, M. *J. Am. Chem. Soc.* **1999**, *121*, 7257. (b) Slowinski, K.; Chamberlain, R. V.; Miller, C. J.; Majda, M. *J. Am. Chem. Soc.* **1997**, *119*, 11910. (c) Slowinski, K.; Slowinski, K.; Majda, M. *J. Phys. Chem. B* **1999**, *103*, 8544.

(14) Chen, J.; Reed, M. A.; Asplund, C. L.; Cassell, A. M.; Myrick, M. L.; Rawlett, A. M.; Tour, J. M.; Van Patten, P. G. *Appl. Phys. Lett.* **1999**, *75*, 624.

(15) Bigioni, T. P.; Harrell, L. E.; Guthrie, D. K.; Cullen, W. G.; Whetten, R. L.; First, P. N. *Eur. Phys. J.* **1999**, *D6*, 355. (b) Fan, F. F.; Yang, J.; Dirk, S. M.; Price, D. W.; Kosynkin, D.; Tour, J. M.; Bard, A. J. *J. Am. Chem. Soc.* **2001**, *123*, 2454.

(16) (a) Chidsey, C. E. D. *Science* **1991**, *251*, 919. (b) Smalley, J. F.; Feldberg, S. W.; Chidsey, C. E. D.; Linford, M. R.; Newton, M. D.; Liu, Y.-P. *J. Phys. Chem.* **1995**, *99*, 13141. (c) Forster, R. J.; Faulkner, L. R. *J. Am. Chem. Soc.* **1994**, *116*, 5455.

(17) (a) Finklea, H. O. Electrochemistry of Organized Monolayers of Thiols and Related Molecules on Electrodes. In *Electroanalytical Chemistry*; Bard, A. J., Rubinstein, I., Eds.; Marcel Dekker: New York, 1996; pp 109−135, and references therein. (b) Hanshaw, D. D.; Finklea, H. O. *J. Am. Chem. Soc.* **1992**, *114*, 3173. (c) Finklea, H. O.; Liu, L.; Ravenscroft, M. S.; Punturi, S. *J. Phys. Chem.* **1996**, *100*, 18852. (d) Weber, K.; Creager, S. E. *Anal. Chem.* **1994**, *66*, 3164. (e) Tender, L.; Carter, M. T.; Murray, R. W. *Anal. Chem.* **1994**, *66*, 3171. (f) Nahir, T. M.; Clark, R. A.; Bowden, E. F. *Anal. Chem.* **1994**, *66*, 2595.

(18) (a) Moses, P. R.; Murray, R. W. *J. Am. Chem. Soc.* **1976**, *98*, 7435. (b) Moses, P. R.; Murray, R. W. *J. Electroanal. Chem.* **1977**, *77*, 393. (c) Murray, R. W. *Acc. Chem. Res.* **1980**, *13*, 135.

(19) Brust, M.; Walker, M.; Bethell, D.; Schiffrin, D. J.; Whyman, R. *Chem. Commun.* **1994**, 801.

(20) Hostetler, M. J.; Templeton, A. C.; Murray, R. W. *Langmuir* **1999**, *15*, 3782.

(21) Hostetler, M. J.; Wingate, J. E.; Zhong, C.-J.; Harris, J. E.; Vachet, R. W.; Clark, M. R.; Londono, J. D.; Green, S. J.; Stokes, J. J.; Wignall, G. D.; Glish, G. L.; Porter, M. D.; Evans, N. D.; Murray, R. W. *Langmuir* **1998**, *14*, 17.

(22) Bard, A. J.; Faulkner, L. R. *Electrochemical Methods*; Wiley: New York, 2000.

(23) The coverage of a monolayer of MPC was determined via quartz crystal microbalance: Cliffel, D. E.; Murray, R. W., unpublished results, UNC−Ch, 2000.

(24) Laviron, E. *J. Electroanal. Chem.* **1979**, *101*, 19.

(25) Values for the graph inset in Figure 2 were extrapolated from a plot generated using data listed in Table 1 of ref 24, which were calculated for $\alpha = 0.5$.

(26) (a) Creager, S. E.; Wooster, T. T. *Anal. Chem.* **1998**, *70*, 4257. (b) Brevnov, D. A.; Finklea, H. O. *Langmuir* **2000**, *16*, 5973. (c) Nahir, T. M.; Bowden, E. F. *J. Electroanal. Chem.* **1996**, *410*, 9.

(27) Experimental data were simulated using the Z-plot ® for windows program.

(28) Zamborini, F. P.; Leopold, M. C.; Hicks, J. F.; Kuleza, P.; Malik, M. A.; Murray, R. W. *J. Am. Chem. Soc.* **2002**, in press.

(29) These estimates are based on a 10^6 s^{-1} rate constant for a 12 carbon unit pathway according to the exponential relation, $k_{ET} \propto \exp[-\beta_n n]$ where β_n the electronic coupling parameter is[16b,17] $\sim$1.1/CH_2 (or CH_3) and n is the number of CH_2 and CH_3 units in the tunneling pathway. The estimate ignores the carboxylate groups and any effects of non trans orientations in the thiolate ligand chains.

(30) DeLevie, R. D. *J. Electroanal. Chem.* **1989**, *261*, 1.